Geophys. J. Int. (2004) **158,** 457–469 doi: 10.1111/j.1365-246X.2004.02281.x

The magnetotelluric phase tensor

T. Grant Caldwell,[1,2] Hugh M. Bibby[1] and Colin Brown[2]

[1] *Institute of Geological and Nuclear Sciences,* PO Box 30368, *Lower Hutt, New Zealand. E-mail: g.caldwell@gns.cri.nz*
[2] *Applied Geophysics Unit, National University of Ireland, Galway, Ireland*

Accepted 2004 February 10. Received 2004 February 10; in original form 2003 February 20

SUMMARY

The phase relationships contained in the magnetotelluric (MT) impedance tensor are shown to be a second-rank tensor. This tensor expresses how the phase relationships change with polarization in the general case where the conductivity structure is 3-D. Where galvanic effects produced by heterogeneities in near-surface conductivity distort the regional MT response the phase tensor preserves the regional phase information. Calculation of the phase tensor requires no assumption about the dimensionality of the underlying conductivity distribution and is applicable where both the heterogeneity and regional structure are 3-D.

For 1-D regional conductivity structures, the phase tensor is characterized by a single coordinate invariant phase equal to the 1-D impedance tensor phase. If the regional conductivity structure is 2-D, the phase tensor is symmetric with one of its principal axes aligned parallel to the strike axis of the regional structure. In the 2-D case, the principal values (coordinate invariants) of the phase tensor are the transverse electric and magnetic polarization phases. The orientation of the phase tensor's principal axes can be determined directly from the impedance tensor components in both 2-D and 3-D situations. In the 3-D case, the phase tensor is non-symmetric and has a third coordinate invariant that is a distortion-free measure of the asymmetry of the regional MT response. The phase tensor can be depicted graphically as an ellipse, the major and minor axes representing the principal axes of the tensor. 3-D model studies show that the orientations of the phase tensor principal axes reflect lateral variations (gradients) in the underlying regional conductivity structure. Maps of the phase tensor ellipses provide a method of visualizing this variation.

Key words: electromagnetic methods, galvanic distortion, magnetotellurics.

INTRODUCTION

In magnetotelluric (MT) surveys localized heterogeneities in conductivity near the Earth's surface distort the electromagnetic (EM) response produced by the underlying or 'regional' conductivity structure under investigation. As the period of the MT signal increases, *inductive* (i.e. period- or frequency-dependent) effects produced by the (localized) near-surface structures decrease and eventually become negligible compared with the inductive response produced by the regional conductivity structure (e.g. Jiracek 1990). Thus for periods greater than some minimum value, which depends on the length scale, geometry and conductivities involved, the distortion produced in the regional EM field is virtually independent of period. Except in unusual cases where the distortion of the regional current density is very severe, the horizontal magnetic field components are not significantly affected and the distortion in the EM field is almost entirely confined to the electric field. Under these conditions, the horizontal components of the observed magnetic field are to a good approximation the same as the corresponding (unperturbed) components of the regional magnetic field.

The distortion of the electric field is caused by the charge formed at the boundaries of the near-surface conductivity heterogeneity by the flux of regional current through the heterogeneity or by the topography near the measurement location (Jiracek 1990). The secondary or scattered electric field produced by the charge distorts the pattern of regional current flow in a localized area encompassing the heterogeneity. For this reason, the frequency-independent distortions of the electric field that are the subject of this paper are termed galvanic distortions. Galvanic distortions are commonly observed in MT surveys and also occur in direct current (DC) resistivity and active-source EM methods that use measurements of the electric field to probe the subsurface (e.g. Caldwell & Bibby 1998; Caldwell *et al.* 2002).

Although the amplitude of the observed electric field may be drastically distorted by a near-surface heterogeneity, the phase relationship between the electric and (horizontal) magnetic field vectors will be virtually unaffected if the distortion is galvanic. That is, the phase relationship will be the same as would be observed in the absence of the distortion. In essence, MT distortion analysis seeks to recover the regional phase relationship from a set of distorted measurements.

The amplitude and phase relationships between the horizontal components of the electric and magnetic fields are represented by a frequency-dependent impedance tensor; a second-rank, two dimensional (2-D) tensor with four complex components. Each component of the impedance tensor can be associated with a phase. However, only where the conductivity distribution has a high degree of symmetry and the impedance tensor has a simple form will the component phases be simply related to the phase difference between linearly polarized components of the horizontal electric and magnetic fields. In situations where the regional response has been distorted, the amplitude and phase of the individual components of the regional impedance tensor will be mixed among the components of the observed impedance tensor complicating the phase relationship between the fields. In this case, or if the regional conductivity structure is 3-D, the electric field response will (in general) be elliptically polarized for a linearly polarized magnetic field.

Previous approaches to MT distortion analysis have all assumed that the regional conductivity structure is either 1-D or 2-D. With this assumption, the amplitude and phase relationships between the horizontal components of the regional EM field can be represented by an impedance tensor with two non-zero components. Reviews of previous approaches to MT distortion analysis can be found in Jiracek (1990), Bruton (1994), Smith (1995), Ritter (1996) and McNeice & Jones (2001). In this paper we will demonstrate how the regional phase information can be recovered directly from the observed impedance tensor where *both* the near-surface heterogeneity and regional conductivity structures are 3-D.

THEORETICAL BACKGROUND

Galvanic distortion

The distortion produced by a localized conductivity heterogeneity on the regional electric field $\mathbf{E}_R$ (i.e. the field that would be observed at the surface in the absence of the heterogeneity) can be represented by the equation

$$\mathbf{E}(\omega) = \mathbf{E}_R(\omega) + \mathbf{E}_S(\omega), \tag{1}$$

where $\mathbf{E}$ is the observed electric field, $\mathbf{E}_S$ is the scattered or secondary electric field produced by the action of the regional field on the conductivity heterogeneity and ω is the angular frequency. Assuming that inductive effects are negligible and that $\mathbf{E}_R$ does not vary significantly over the lateral extent of the conductivity heterogeneity (Groom & Bahr 1992; Chave & Smith 1994) the scattered field $\mathbf{E}_S$ is to a good approximation linearly proportional to the regional electric field $\mathbf{E}_R$. With these assumptions eq. (1) may be rewritten in terms of a frequency-independent linear operator or distortion matrix ($\mathbf{D}$) that maps the regional electric field vector into the distorted field $\mathbf{E}$ observed at the surface. That is

$$\mathbf{E}(\omega) = \mathbf{D}\mathbf{E}_R(\omega), \tag{2}$$

where the 2×2 matrix $\mathbf{D}$ (a second rank, 2-D tensor) is real. This is equivalent to saying that the observed electric field is a linear superposition of the regional field and a scattered electric field ($\mathbf{E}_S$) that is *in-phase* with the regional field (e.g. Bahr 1988, 1991). Note that since $\mathbf{D}$ is real, if the regional electric field is linearly polarized the distorted electric field is also linearly polarized although not usually in the same direction.

In a Cartesian coordinate system (x_1, x_2) the distortion tensor can be written as the matrix

$$\mathbf{D} = \begin{bmatrix} d_{11} & d_{12} \\ d_{21} & d_{22} \end{bmatrix}, \tag{3}$$

where the components d_{ij} depend on the position of the observation point, the shape of the heterogeneity and its conductivity; all of which are unknown.

In situations where eq. (2) is valid, the horizontal components of the observed magnetic field, denoted by $\mathbf{H}$ throughout this paper, are (to a good approximation) equal to the corresponding components of the regional field $\mathbf{H}_R$ and

$$\mathbf{H}(\omega) = \mathbf{H}_R(\omega). \tag{4}$$

The conditions under which eqs (2) and (4) are good approximations are discussed in Groom & Bahr (1992), Singer (1992), Chave & Smith (1994) and Utada & Munekane (2000).

Impedance tensor

The amplitude and phase relationships between the horizontal components of the EM field observed at the surface are represented by the impedance tensor $\mathbf{Z}$ defined by the relationship

$$\mathbf{E}(\omega) = \mathbf{Z}(\omega)\mathbf{H}(\omega). \tag{5}$$

In general (i.e. where the conductivity distribution is 3-D), $\mathbf{Z}$ is a non-symmetric tensor and can be thought of as a (complex) linear operator that transforms a linearly polarized magnetic field into an elliptically polarized electric field. The regional impedance tensor is similarly defined i.e.

$$\mathbf{E}_R(\omega) = \mathbf{Z}_R(\omega)\mathbf{H}_R(\omega). \tag{6}$$

Galvanic distortion of the impedance tensor

Assuming that a galvanic distortion is present then (from eqs 2, 3, 5 and 6)

$$\mathbf{E} = \mathbf{D}\mathbf{E}_R = \mathbf{D}(\mathbf{Z}_R\mathbf{H}_R) = (\mathbf{D}\mathbf{Z}_R)\mathbf{H} \tag{7}$$

and thus the relationship between the observed (distorted) and regional impedance tensors is

$$\mathbf{Z} = \mathbf{D}\mathbf{Z}_R. \tag{8}$$

Separating the complex impedance tensors into their real ($\mathbf{X}$) and imaginary ($\mathbf{Y}$) parts, we can write:

$$\mathbf{Z} = \mathbf{X} + i\mathbf{Y} \tag{9}$$

and

$$\mathbf{Z}_R = \mathbf{X}_R + i\mathbf{Y}_R. \tag{10}$$

Thus, from eq. (8):

$$\mathbf{X} = \mathbf{D}\mathbf{X}_R \tag{11}$$

and

$$\mathbf{Y} = \mathbf{D}\mathbf{Y}_R. \tag{12}$$

Since $\mathbf{D}$ is unknown the amplitude information contained in $\mathbf{Z}_R$ cannot be recovered from $\mathbf{Z}$ without other independent information (e.g. Smith 1995). However, since $\mathbf{D}$ is real the essential phase relationship between the horizontal components of the regional electric and magnetic fields must be unaffected by the distortion. It is the nature and determination of the phase relationship in a situation where the conductivity structure is 3-D that is addressed below.

PHASE TENSOR

Definition

The phase of a complex number is defined from the ratio of its real and imaginary parts. This relationship can be generalized to a complex matrix or tensor. Hence, we define the phase tensor by the relation

$$\mathbf{\Phi} = \mathbf{X}^{-1}\mathbf{Y}, \tag{13}$$

where $\mathbf{X}^{-1}$ (a tensor) is the inverse of $\mathbf{X}$ and $\mathbf{\Phi}$ is real. (Formally, eq. (13) is a particular contraction of the tensor product of $\mathbf{X}^{-1}$ and $\mathbf{Y}$.) The relationship between the phase tensors of the observed and regional impedance tensors can be derived directly from eqs (11) and (12), i.e.

$$\begin{aligned}\mathbf{\Phi} &= \mathbf{X}^{-1}\mathbf{Y} \\ &= (\mathbf{D}\mathbf{X}_\mathrm{R})^{-1}(\mathbf{D}\mathbf{Y}_\mathrm{R}) \\ &= \mathbf{X}_\mathrm{R}^{-1}\mathbf{D}^{-1}\mathbf{D}\mathbf{Y}_\mathrm{R} = \mathbf{X}_\mathrm{R}^{-1}\mathbf{Y}_\mathrm{R} \\ &= \mathbf{\Phi}_\mathrm{R}.\end{aligned} \tag{14}$$

Thus the observed and regional phase tensors are identical and are independent of the distortion tensor, consistent with the behaviour expected for the phase on physical grounds. Note, no assumption about the nature or dimensionality of the regional conductivity structure is required and eq. (14) is applicable where the conductivity structure is 3-D.

Written in terms of the real and imaginary components of $\mathbf{Z}$ in a Cartesian coordinate system (x_1, x_2), the phase tensor $\mathbf{\Phi}$ can be written as the matrix

$$\begin{bmatrix}\Phi_{11} & \Phi_{12} \\ \Phi_{21} & \Phi_{22}\end{bmatrix} = \frac{1}{\det(\mathbf{X})}\begin{bmatrix}X_{22}Y_{11} - X_{12}Y_{21} & X_{22}Y_{12} - X_{12}Y_{22} \\ X_{11}Y_{21} - X_{21}Y_{11} & X_{11}Y_{22} - X_{21}Y_{12}\end{bmatrix}, \tag{15}$$

where $\det(\mathbf{X}) = X_{11}X_{22} - X_{21}X_{12}$ is the determinant of $\mathbf{X}$. Note that, in general, $\mathbf{\Phi}$ will be non-symmetric and that, the components of $\mathbf{\Phi}$ are *not* functions of the impedance tensor arguments (component phases) alone, i.e. $\Phi_{ij} \neq f(\arg[Z_{kl}])$.

Properties in 1-D

If the regional conductivity structure is both isotropic and 1-D (i.e. the conductivity varies only with depth), the impedance tensor in a Cartesian coordinate system (x_1, x_2) has the form

$$\mathbf{Z} = \begin{bmatrix}0 & Z_{12} \\ Z_{21} & 0\end{bmatrix} = \begin{bmatrix}0 & Z_{1\mathrm{D}} \\ -Z_{1\mathrm{D}} & 0\end{bmatrix}, \tag{16}$$

where $Z_{1\mathrm{D}} = X_{1\mathrm{D}} + iY_{1\mathrm{D}} = |Z_{1\mathrm{D}}|\,\mathrm{e}^{i\phi}$ and

$$\phi = \tan^{-1}(Y_{1\mathrm{D}}/X_{1\mathrm{D}}). \tag{17}$$

Thus (from eq. 15)

$$\mathbf{\Phi}_{1\mathrm{D}} = \begin{bmatrix}Y_{1\mathrm{D}}/X_{1\mathrm{D}} & 0 \\ 0 & Y_{1\mathrm{D}}/X_{1\mathrm{D}}\end{bmatrix} = (Y_{1\mathrm{D}}/X_{1\mathrm{D}})\mathbf{I} = \tan(\phi)\mathbf{I} \tag{18}$$

where $\mathbf{I}$ is the identity matrix, and $\mathbf{\Phi}$ is characterized by a single scalar quantity equal to the tangent of the conventional MT phase for a 1-D structure. Note that the tensor form in eq. (18) is invariant under rotation; i.e. the regional electric and magnetic fields are perpendicular and independent of the direction of polarization.

Coordinate invariants

Just as a vector is characterized by its direction and magnitude, a real second-rank, 2-D tensor is characterized (in the general case) by a direction and three independent scalar quantities that are independent of the coordinate system used to express the tensor, i.e. by three coordinate invariants. Since any function of the invariants is also coordinate invariant many different ways of expressing the invariants are possible. In this paper we will adopt one of the representations used by Bibby (1986) in his analysis of the DC apparent resistivity tensor. The coordinate invariants that we will use are the maximum ($\Phi_{\max}$) and minimum ($\Phi_{\min}$) tensor values, simple functions of the tensor components given in the Appendix, and the skew angle β given by the expression

$$\beta = \frac{1}{2}\tan^{-1}\left(\frac{\Phi_{12} - \Phi_{21}}{\Phi_{11} + \Phi_{22}}\right). \tag{19}$$

This angle can be thought of as a rotation and is a measure of the tensor's asymmetry. Note that β depends on the tensor's skew $(\Phi_{12} - \Phi_{21})$, which is invariant under rotation but changes sign if the coordinate system is reflected.

Principal or singular value decomposition

Expressed in terms of these quantities, the phase tensor can be written in the form:

$$\mathbf{\Phi} = \mathbf{R}^{\mathrm{T}}(\alpha - \beta)\begin{bmatrix}\Phi_{\max} & 0 \\ 0 & \Phi_{\min}\end{bmatrix}\mathbf{R}(\alpha + \beta), \tag{20}$$

where $\mathbf{R}(\alpha + \beta)$ is the rotation matrix

$$\mathbf{R}(\alpha + \beta) = \begin{bmatrix}\cos(\alpha + \beta) & \sin(\alpha + \beta) \\ -\sin(\alpha + \beta) & \cos(\alpha + \beta)\end{bmatrix}, \tag{21}$$

$\mathbf{R}^{\mathrm{T}}$ is the transposed or inverse rotation matrix, i.e. $\mathbf{R}^{\mathrm{T}}(\theta) = \mathbf{R}^{-1}(\theta) = \mathbf{R}(-\theta)$, and

$$\alpha = \frac{1}{2}\tan^{-1}\left(\frac{\Phi_{12} + \Phi_{21}}{\Phi_{11} - \Phi_{22}}\right). \tag{22}$$

This angle expresses the tensor's dependence on the coordinate system and with the three coordinate invariants completely defines the tensor. Note that eq. (20) has the same form as the singular value decomposition (SVD) of a square matrix (e.g. Press *et al.* 1986). Thus, the maximum and minimum values $\Phi_{\max}$ and $\Phi_{\min}$ are the principal or singular values of $\mathbf{\Phi}$. Since the SVD parameters have explicit forms (eqs 19, 22, A8 and A9) their standard errors can be determined explicitly if the variances and covariances of the impedance tensor components are known.

The invariance of the principal values and skew angle can be demonstrated by rotating the Cartesian coordinate system used to express the tensor. Rotating by an angle θ,

$$\begin{aligned}\mathbf{R}(\theta)\mathbf{\Phi}\mathbf{R}^{\mathrm{T}}(\theta) &= \mathbf{R}(\theta)\mathbf{R}^{\mathrm{T}}(\alpha - \beta)\begin{bmatrix}\Phi_{\max} & 0 \\ 0 & \Phi_{\min}\end{bmatrix}\mathbf{R}(\alpha + \beta)\mathbf{R}^{\mathrm{T}}(\theta) \\ &= \mathbf{R}^{\mathrm{T}}(\alpha - \theta - \beta)\begin{bmatrix}\Phi_{\max} & 0 \\ 0 & \Phi_{\min}\end{bmatrix}\mathbf{R}(\alpha - \theta + \beta) \\ &= \mathbf{R}^{\mathrm{T}}(\alpha' - \beta)\begin{bmatrix}\Phi_{\max} & 0 \\ 0 & \Phi_{\min}\end{bmatrix}\mathbf{R}(\alpha' + \beta)\end{aligned} \tag{23}$$

where $\alpha' = (\alpha - \theta)$. The net effect of the rotation is to change the angle α to the angle α', all other parameters are unchanged i.e. coordinate invariant.

If the phase tensor is symmetric ($\beta = 0$) the principal values of the tensor are equal to its eigenvalues. This situation occurs where the regional conductivity distribution is mirror symmetric, e.g. where the regional conductivity distribution is 1-D or 2-D. Where $\mathbf{\Phi}$ is symmetric and has equal principal values, such as is the case if the conductivity distribution is uniform or 1-D, the electric field will be linearly polarized if the magnetic field is linearly polarized. In the 2-D case, the principal values will usually be distinct (i.e. $\Phi_{\max} \neq \Phi_{\min}$) and there will be two directions for which a linearly polarized magnetic field will give rise to a linearly polarized electric field. If the 2-D response is not distorted these two directions will be orthogonal. In all other directions the electric field will be elliptically polarized.

Graphical representation

Any second-rank, non-symmetric 2-D tensor can be represented graphically by an ellipse (e.g. Bibby 1986) and the quantities in eq. (20) have simple interpretations in terms of the properties of the tensor ellipse illustrated in Fig. 1. In particular, the major and minor axes of the ellipse depict the principal axes and values of the tensor with the orientation of the major axis specified by the angle $\alpha - \beta$. Note that where the phase tensor is symmetric (i.e. $\beta = 0$) the orientation of the major axis is given by α. In the general (3-D) case, the skew angle (β) is non-zero and represents the rotation of the major axis of the phase tensor ellipse away from an identically shaped ellipse represented by a symmetric tensor. A simple method of constructing the tensor ellipse is described in the Appendix.

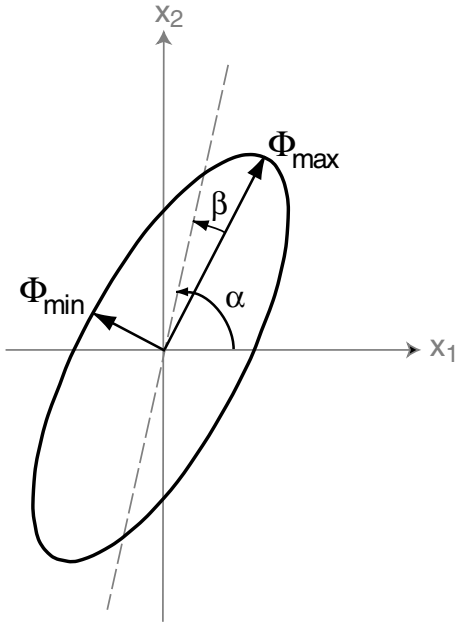

Figure 1. Graphical representation of the phase tensor. The lengths of the ellipse axes, which represent the principal axes of the tensor, are proportional to the principal (or singular) values of the tensor. If the phase tensor is non-symmetric, a third coordinate invariant represented by the angle β is needed to characterize the tensor. The direction of the major axis of the ellipse, given by the angle $\alpha - \beta$, defines the relationship of the tensor to the observer's reference frame or coordinate system (x_1, x_2).

Tensor ellipse in 1-D

The simplest example of this representation is the tensor ellipse for a uniform conductivity half-space. In this case, a circle of unit radius represents the phase tensor at all periods. More generally, if the conductivity is both isotropic and 1-D, the radius of the circle will vary with period according to the variation of the conductivity with depth. For example, the radius will increase if the conductivity increases with depth. In the 1-D case, or in a situation where the conductivity distribution is cylindrically symmetric about the measurement point, α is undefined. In practice this means that if the conductivity is 1-D the value of α will be unstable due to noise in the observed data. Whether or not α is significant within the uncertainties of the observed (and perhaps distorted) data may be tested using the expected properties of the phase tensor invariants as significance criteria. In particular, if the difference in the lengths of the major and minor axes ($\Phi_{\max} - \Phi_{\min}$) is less than the corresponding standard error then α is insignificant and the tensor ellipse is indistinguishable from a circle.

Anisotropic half-space

Where a half-space has a uniform but horizontally anisotropic conductivity (i.e. where one of the principal axes of the conductivity tensor is aligned vertically) the conductivity is mirror symmetric about the horizontal principal axes and the phase tensor skew angle $\beta = 0$. In a Cartesian coordinate system with axes aligned with the principal axes of the conductivity tensor, the impedance tensor has an antidiagonal form. However, in contrast to an isotropic half-space (eq. 16), the magnitudes of the off-diagonal components of the impedance tensor for the anisotropic case are different. Consequently, the amplitude of the electric field will vary as the direction of the magnetic field polarization changes but the phase difference between the electric and magnetic fields will not. Thus, the phase tensor is also represented by a unit circle ($\mathbf{\Phi} = \mathbf{I}$) in the case of a uniform horizontally anisotropic half-space. This means that if the magnetic field is linearly polarized, the electric field is also linearly polarized but will be perpendicular to the magnetic field only where the polarization directions coincide with the directions of the principal axes of the conductivity tensor.

In a horizontally layered situation where an isotropic layer (or layers) overlies an anisotropic half-space, any difference (or split) between the principal phases is a consequence of the conductivity contrast at the boundary between the isotropic and anisotropic material and is not directly indicative of the underlying anisotropy of the half-space. Thus information pertaining directly to the anisotropy can only be obtained from the amplitude of the MT response. In practice, the difficulty is that the amplitude response may have been distorted by structure at length scales less than the depth of the anisotropic layer. More generally, the observation of a phase split between the principal phase values indicates that a conductivity gradient (lateral or vertical) exists, nothing more.

Properties in 2-D

In the 2-D case (the assumption made in previous approaches to MT distortion analysis) the strike of the regional conductivity distribution defines a natural orientation for the coordinate system. In a Cartesian coordinate system (x_1', x_2') aligned with x_1' parallel to the (unknown) strike direction, at say an angle θ with respect to the observation coordinate system, the regional impedance tensor $\mathbf{Z}_{\mathrm{R}}'$

has the antidiagonal form:

$$\mathbf{Z}'_{\mathrm{R}} = \begin{bmatrix} 0 & Z'_{12} \\ Z'_{21} & 0 \end{bmatrix} = \begin{bmatrix} 0 & Z_{\parallel} \\ -Z_{\perp} & 0 \end{bmatrix}, \tag{24}$$

where quantities in the rotated coordinate system are denoted by a prime ($'$) and $Z_{\parallel}$ and $Z_{\perp}$, are the transverse electric (TE) and transverse magnetic (TM) impedance respectively. That is, $Z_{\parallel}$ and $Z_{\perp}$ are the impedances measured when the electric field is linearly polarized parallel or perpendicular to the strike of the conductivity distribution. The antidiagonal form of the impedance tensor expresses the orthogonality of the electric and magnetic fields where the fields are polarized parallel or perpendicular to the strike of the conductivity structure.

Rotating the observed phase tensor $\mathbf{\Phi}$ by the unknown angle θ, the phase tensor in the rotated coordinate system is given by

$$\begin{aligned} \mathbf{\Phi}' &= \mathbf{R}(\theta)\mathbf{\Phi}\mathbf{R}^{\mathrm{T}}(\theta) \\ &= \left[\mathbf{R}(\theta)\mathbf{X}_{\mathrm{R}}^{-1}\mathbf{R}^{\mathrm{T}}(\theta)\right]\left[\mathbf{R}(\theta)\mathbf{Y}_{\mathrm{R}}\mathbf{R}^{\mathrm{T}}(\theta)\right] \\ &= (\mathbf{X}'_{\mathrm{R}})^{-1}\mathbf{Y}'_{\mathrm{R}}. \end{aligned} \tag{25}$$

Since $\mathbf{Z}'_{\mathrm{R}}$ is antidiagonal so are $\mathbf{X}'_{\mathrm{R}}$ and $\mathbf{Y}'_{\mathrm{R}}$. Thus, the inverse tensor $(\mathbf{X}'_{\mathrm{R}})^{-1}$ is also antidiagonal. Hence, the matrix product $(\mathbf{X}'_{\mathrm{R}})^{-1}\,\mathbf{Y}'_{\mathrm{R}}$ is diagonal and the phase tensor in the rotated coordinate system has the diagonal form:

$$\mathbf{\Phi}' = \begin{bmatrix} Y_{\perp}/X_{\perp} & 0 \\ 0 & Y_{\parallel}/X_{\parallel} \end{bmatrix} \text{ or } \begin{bmatrix} Y_{\parallel}/X_{\parallel} & 0 \\ 0 & Y_{\perp}/X_{\perp} \end{bmatrix}. \tag{26}$$

Comparing $\mathbf{\Phi}'$ (eq. 26) with the SVD form in eq. (20), it can be seen that the phase tensor coordinate invariants are $Y_{\perp}/X_{\perp}$, $Y_{\parallel}/X_{\parallel}$ and $\beta = 0$. The principal values of the phase tensor for 2-D conductivity distribution are thus the tangents of the corresponding conventional TM and TE polarization phases. Note that the condition $\beta = 0$ is a necessary but not sufficient condition for a 2-D regional conductivity structure. For a 2-D structure, β must be zero at all periods greater than the minimum value for which the galvanic approximation applies. In practice, what we seek is a range of frequencies where β is zero (within the observational errors) and the direction of the phase tensor major axis is constant.

Since $\beta = 0$ in the 2-D case, the orientation of the major axis of the phase tensor ellipse in the rotated coordinate system is given by the angle α'. Thus from eqs (22) and (26), $\alpha' = 0^{\circ}$ and the major axis of the phase tensor ellipse is aligned parallel or perpendicular to the strike of the (regional) conductivity distribution. In the observer's frame of reference (i.e. in the unrotated coordinate system) the orientation of strike axis is $\alpha = \theta$ or $\alpha = \theta + 90^{\circ}$. The 90° ambiguity remains since (*a priori*) we have no knowledge as to which of the maximum or minimum phases corresponds to the TE or TM polarization. (In practice, the ambiguity is resolved using vertical magnetic field data.) Note that, if the regional conductivity structure is 2-D, eq. (22) is an explicit expression for the direction (α) of the strike axis (or its normal), irrespective of whether or not the response has been galvanically distorted.

Galvanic distortion of a 2-D response

If the regional conductivity structure is 2-D there are two directions for which a linearly polarized magnetic field will give rise to a linearly polarized electric field. A galvanic distortion will not change the polarization state of the EM field so that there are also two directions where the observed (distorted) electric and magnetic fields are both linearly polarized. Although the distortion will usually change the direction of regional electric field polarization, the corresponding direction of the magnetic field will be virtually unaffected provided that the distortion of the regional current density does not significantly distort the magnetic field components (i.e. eq. 4 is a good approximation). The problem of determining the 2-D strike direction from the distorted data is thus equivalent to identifying the direction of a linearly polarized magnetic field for which the electric field is also linearly polarized. This direction defines the strike direction of the regional conductivity structure or its normal.

The effect of a galvanic distortion on the response of a regional 2-D conductivity distribution is illustrated in Fig. 2 using ellipses to represent all of the tensors involved. The case illustrated is a synthetic example taken from McNeice & Jones (2001). Note that rotating Fig. 2 leaves the configuration of the ellipses unchanged; only the angle specifying the orientation of the diagram with respect to the observer changes. The lengths of the ellipse axes, their relative orientation with respect to each other and their orientation with respect to the conductivity distribution (i.e. with respect to the Earth) do not depend on the particular frame of reference chosen. It is these quantities (the coordinate invariants) that express the essential physical relationship between the conductivity distribution and the EM field observations.

Fig. 2(a) shows the phase tensor derived from the real (solid) and imaginary (dotted) parts of distorted impedance tensor (Fig. 2b). Note that the orientations of the principal axes of the phase tensor are the same as the major and minor axes of the ellipses that represent the real and imaginary parts of the regional impedance tensor (Fig. 2d). This set of axes defines the strike axes of the regional conductivity structure, i.e. the directions in which a linearly polarized regional magnetic field give rise to a linearly polarized electric field. These ellipses, and the ones used in Fig. 2(b) to represent the observed impedance, are (polar) plots of the electric field magnitudes $|\Re\mathbf{E}|$ and $|\Im\mathbf{E}|$ produced by a unit-magnitude linearly polarized magnetic field drawn in the direction of the corresponding electric field vector (e.g. Bibby 1986; Caldwell *et al.* 2002; Appendix A).

This method of graphically representing the impedance tensor has the advantage that the two sets of principal axes that characterize the (complex) impedance tensor can be simply and directly depicted. For example, if the regional conductivity structure is 2-D the major axes of both $\mathbf{X}_{\mathrm{R}}$ and $\mathbf{Y}_{\mathrm{R}}$ must be parallel or perpendicular to the conductivity structure as is illustrated in Fig. 2(d). This requirement can also be expressed as a condition on the skew angles (β_{X} and β_{Y}) and on the angle between the major axes of the two ellipses representing the regional impedance tensor. All of these quantities are coordinate invariant. Since the traces (another coordinate invariant form) of $\mathbf{X}_{\mathrm{R}}$ and $\mathbf{Y}_{\mathrm{R}}$ are zero in 2-D (eq. 24), the skew angles β_{X} and β_{Y} have values of $\pm 45^{\circ}$. In the Cartesian coordinate system with axes parallel to the strike axes, the diagonal terms of the impedance tensor are both zero and $\alpha'_{\mathrm{X}} = \pm\,45^{\circ}$ and $\alpha'_{\mathrm{Y}} = \pm\,45^{\circ}$. Thus the condition on the angle between the major axes of the real and imaginary parts reduces to the condition that $\alpha'_{\mathrm{X}} = \alpha'_{\mathrm{Y}}$ or $\alpha'_{\mathrm{X}} = \alpha'_{\mathrm{Y}} \pm 90^{\circ}$.

The ellipse representing the distortion tensor in Fig. 2(c) is a polar plot of the magnitude ratio $|\mathbf{E}|/|\mathbf{E}_{\mathrm{R}}|$ in the direction of the observed electric field $\mathbf{E}$. The effect of the distortion tensor on the regional impedance tensor (Fig. 2d) is to amplify or attenuate the principal values of $\mathbf{X}_{\mathrm{R}}$ and $\mathbf{Y}_{\mathrm{R}}$ by different amounts and to reorient the principal axes. Thus two distinct sets of principal axes are needed to characterize the observed impedance tensor as shown in Fig. 2(b). This characteristic is indicative of a 3-D conductivity distribution,

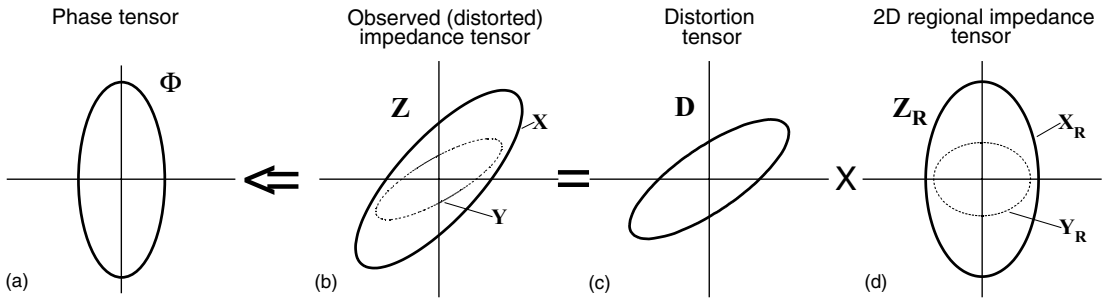

Figure 2. Graphical representation of the tensors involved in the galvanic distortion of a 2-D impedance tensor. The coordinate axes shown are aligned parallel and perpendicular to the strike of the 2-D conductivity structure. The phase tensor, represented by the ellipse shown in (a), is derived from the real (solid line) and imaginary (dotted line) parts of the distorted impedance tensor shown in (b). These ellipses (b) represent the distortion of the 2-D regional impedance tensor (d), characterized by a single set of principal axes aligned with conductivity structure, by the distortion tensor represented by the ellipse shown in (c).

either in the neighbourhood of the measurement site or regionally. Only where further analysis shows that the phase tensor skew angle (β) is insignificant for all periods greater than some minimum value can we infer that the regional conductivity structure is 2-D, and thus that the observed response has been distorted by a localized conductivity heterogeneity.

Properties in 3-D

We will demonstrate the properties of the phase tensor in 3-D using synthetic data calculated with the modelling code described in Xiong (1992) and Xiong & Tripp (1995). The model used for this demonstration (Fig. 3) consists of a small conductive (10 Ω m) cube situated near the surface and a much larger (regional) conductive (1 Ω m) body at depth both embedded in a 100 Ω m half-space. The cube is situated near the corner of the rectangular body in the area where 3-D effects are expected to be large. Maps of the phase tensor ellipses at three different periods (0.0316, 0.316 and 3.16 s) with contours showing the direction of the major axes and skew angle (β) are shown in Figs 4 and 5, respectively.

Where the difference in the lengths of ellipse axes (Φ_{max} and Φ_{min}) is less than 2 per cent of their corresponding geometric mean (i.e. of the radius of a circle with the same area as the ellipse), the ellipses in Fig. 4 have been left unfilled. At these locations, where the phase tensor is indistinguishable from a circle, the azimuth calculation is potentially unreliable (unstable) because of the limitations in the accuracy of the forward modelling code.

At short periods the MT response will be unaffected by the deep conductor and the observed response will reflect the influence of the near-surface body alone. This can be seen in the phase tensor response (Fig. 4a) as a radial alignment of the major axes around the conductive cube. If the cube is resistive (not shown) rather than conductive the phase tensor ellipses are oriented tangentially. This change in the orientation of the principal axes suggests that the direction of the major axes indicates the preferred flow direction of the induction current.

Support for this interpretation is provided by the induction arrows (Parkinson 1962) also shown in Fig. 4. These arrows are graphical representations of the real part of the vertical magnetic field transfer function or tipper vector (**K**) defined by the equation

$$H_z = -\mathbf{K}\cdot\mathbf{H}, \tag{27}$$

where H_z is the vertical component of the *total* magnetic field and **H** is the horizontal magnetic field vector. In situations where the conductivity distribution varies laterally, the real part of the tipper vector will point towards the region of highest conductance. At

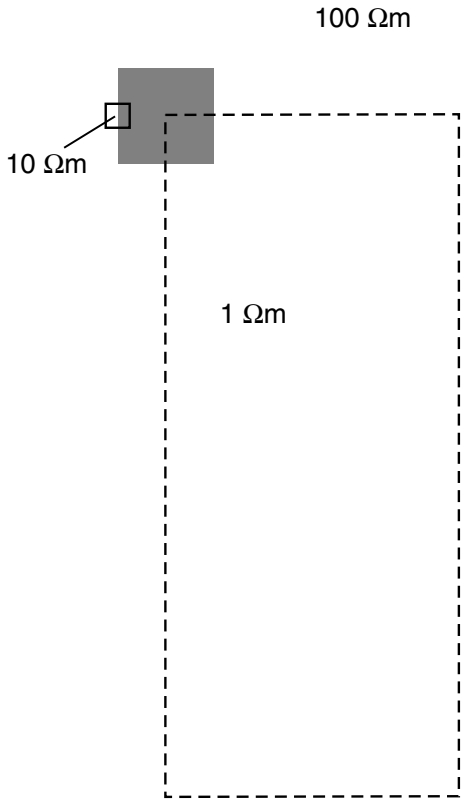

Figure 3. Map view of the conductivity model used to illustrate the properties of the phase tensor in a 3-D situation. The model consists of a small conductive (10 Ω m) cube, sides 0.250 km, with its top 50 m below the surface and a much larger rectangular 1 Ω m body ($7 \times 3 \times 3$ km^3) buried 1.5 km below the surface. Both bodies are embedded in a 100 Ω m half-space. The grey area shows the region covered by the tensor ellipse maps in Figs 4 and 5.

short periods (Fig. 4a), outside the immediate vicinity of the cube, where the conductance sensed by the EM field will be approximately cylindrically symmetric, the induction arrows and major axes of the phase tensor are parallel, consistent with the interpretation of the principal axes of the phase tensor suggested above.

At intermediate periods (Fig. 4b) the alignments of the major axes reflect a mixture of the effects of both the near-surface and deep conductors. At long periods (Fig. 4c), inductive effects produced by the cube are insignificant and the deep conductor dominates the phase response, the alignment of the major axes indicating the

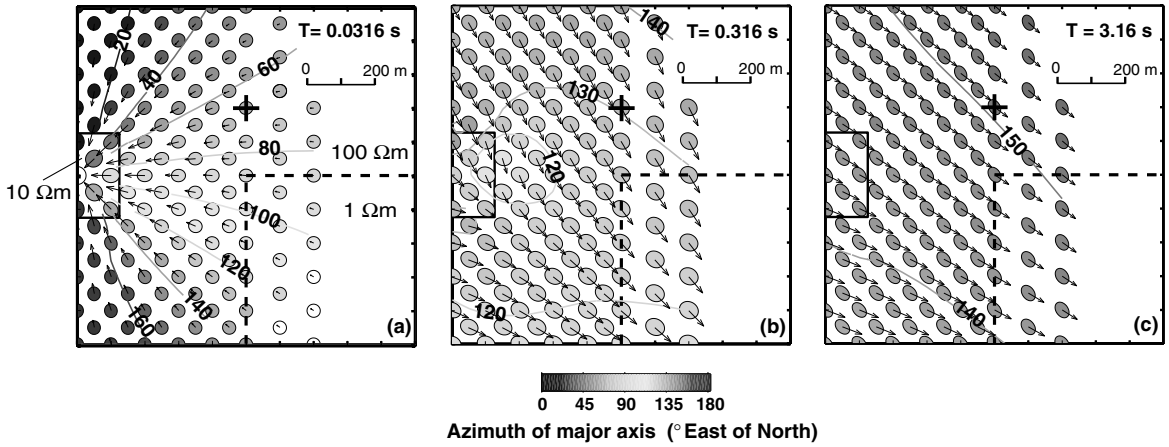

Figure 4. Phase tensor ellipse map and induction arrows (real part) at three different periods for the model shown in Fig. 3. Contours and grey tone filling the ellipses indicate the azimuth of the tensor ellipse major axes.

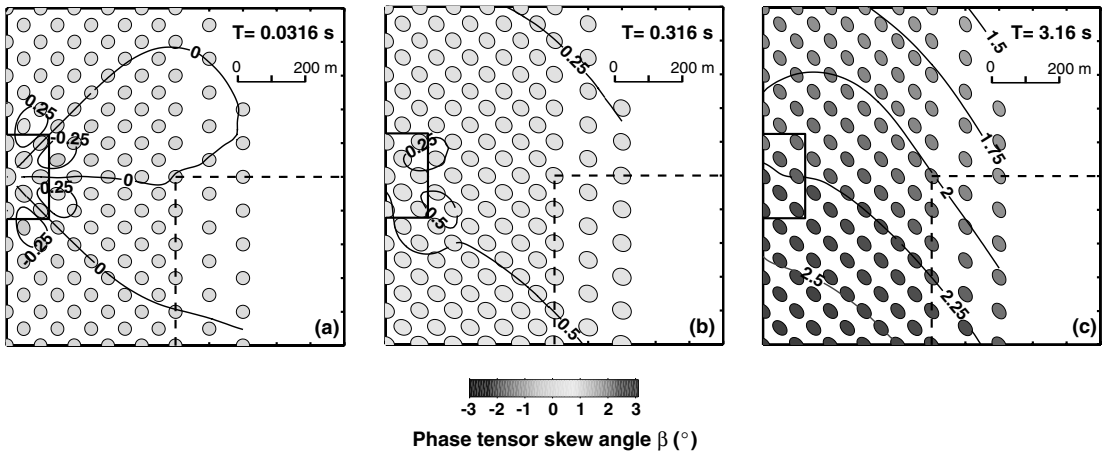

Figure 5. Phase tensor ellipse map at three different periods for the model shown in Fig. 3. Contours and grey tone filling the ellipses show the phase tensor skew angle β.

preferred flow direction of the inductive current associated with the deep conductor. Note that the direction of the ellipse major axes at long periods (Fig. 4c) changes rapidly (approximately 10° in 0.5 km) in a northwest–southeast direction. A rapid lateral change in direction of the principal axes of the phase tensor is a clear indication of a 3-D (regional) conductivity structure.

The corresponding maps of the phase tensor skew angle (β) are shown in Fig. 5. At short periods (Fig. 5a) the skew angle is zero on the cube's axes of symmetry and greatest (although still small, about 0.25°) near the corners of the cube where the conductivity distribution is asymmetrically distributed around the measurement point. At intermediate periods, where the combined effects of both bodies are significant, the variation of the skew angle is more complicated (Fig. 5b) reflecting the asymmetric configuration of both bodies with respect to the measurement point. At longer periods (Fig. 5c) the influence of the near-surface body is insignificant and the skew angle reflects the effect of the deep conductor alone.

Note that at longer periods the ellipse major axis and the induction arrows (Figs 4b and c) are not as closely aligned as they are at short periods (Fig. 4a). This misalignment reflects the asymmetry of the 3-D response at longer periods, which is expressed in the phase tensor as a non-zero skew angle (Figs 5b and c).

Fig. 6 shows graphs of the phase tensor properties as a function of period at the location marked by the cross in Fig. 4. To simulate the effect of noise, an ensemble of 1000 impedance tensors was created by adding 2 per cent Gaussian noise to each component of the calculated impedance tensor. The error bars in Fig. 6 show the standard deviation from the mean value (points) of the corresponding tensor property derived from this ensemble. For periods less than 0.1 s the maximum and minimum phases (Fig. 6a), i.e. $\tan^{-1}(\Phi_{max})$ and $\tan^{-1}(\Phi_{min})$, are close to 45° indicating that the effect of the conductive cube at this location is small. For periods between about 0.1 and 3 s, the phase difference or split between the principal phases increases rapidly as the influence of the inductive currents in the deep conductor becomes dominant. At periods >3 s, the phase split decreases as the induction currents associated with the deep conductor weaken.

Note that the magnitude of the phase difference between the principal phase values is reflected in the size of the error bars for the direction of the major axis (Fig. 6b). In particular the uncertainties are large for periods <0.3 s where the phase difference is small (<3°). Despite the large uncertainty, the direction of maximum inductive current flow associated with each of the conducting bodies at short (Fig. 4a) and long periods (Fig. 4c) can clearly be distinguished in Fig. 6(b). In particular, for periods between 0.3 s and 30 s (where the difference between the principal phases is large) the azimuth of the major axis can be determined within ±5°. At points where the error bars of the principal phases overlap (enclosed by a

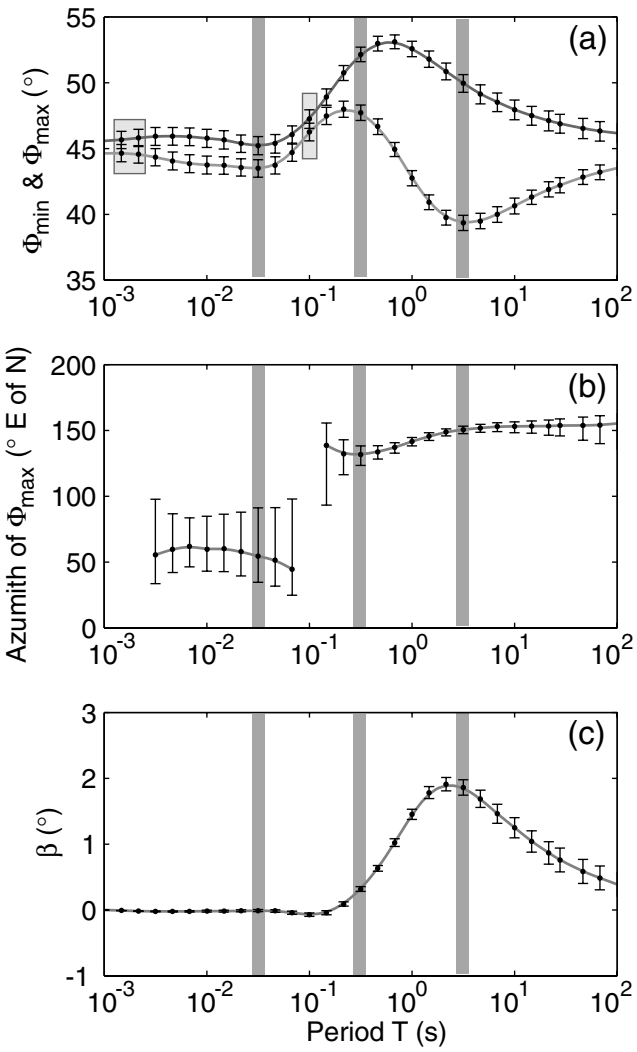

Figure 6. Plots of the phase tensor properties versus period are shown for the location marked by a cross in Fig. 4. The error bars show the standard deviation caused by the addition of synthetic Gaussian noise to the calculated impedance tensor. The periods corresponding to the ellipse maps shown in Figs 4 and 5 are marked in grey. (a) Maximum and minimum phase values. The grey rectangles enclose the points for which the error bar of the maximum and minimum phase values overlap. (b) Azimuth of the tensor ellipse major axis. Points for which the tensor ellipse is indistinguishable from a circle and the azimuth is ill defined are not plotted. (c) Phase tensor skew angle β.

small grey boxes in Fig. 6(a)) the tensor ellipse is indistinguishable from a circle. At these points, omitted from Fig. 6(b), the azimuth is ill-defined. Note that the large uncertainty in the direction ($\alpha - \beta$) of the major axis in Fig 6(b) at periods <0.1 s is a consequence of the small phase difference and thus the uncertainty in the angle α rather than the uncertainty in the skew angle (β), Fig. 6(c).

For the model used in this example β is small ($< 3^\circ$) at all periods and at all locations (Fig. 5). Although small, β is well-determined as shown by the small error bars in Fig. 6(c). Between 0.3 s and 1 s, where β (Fig. 6c) begins to increase and the direction (Fig. 6b) of the major axis varies slightly with period, inductive effects produced by the deep conductor start to become significant. Note that at longer periods (>3 s), where the skew angle begins to decrease, the direction of the major axis (Fig. 6b) remains nearly constant.

DISCUSSION

Geoelectric strike

If the regional conductivity structure is 3-D and the phase difference between the principal values is large enough so that the orientation of the phase tensor principal axes can be determined reliably, a single (well-defined) direction can be associated with the MT phase response at each period. As is illustrated in Fig. 4, the orientations of the major axes of the phase tensor indicate the preferred flow direction of the induction current in a similar fashion to the induction arrows. In particular, if the regional conductivity structure is 2-D, the principal axes of the phase tensor are aligned with the strike axis of the regional conductivity structure. The orientation of the principal axes of the phase tensor can thus be considered to be a generalization of the concept of strike direction (the so-called geoelectric strike) to a 3-D situation. In essence, the principal axes of the phase tensor indicate the (horizontal) directions of the maximum and minimum induction current, which in turn reflect lateral variations in the underlying regional conductivity.

2-D versus 3-D interpretation

In the example illustrated in Fig. 4(c), the direction of the principal axes of the phase tensor at periods >3 s is nearly constant along lines running northwest–southeast. For a single northwest–southeast line of measurements, the MT response will appear to be nearly 2-D. That is, two nearly perpendicular polarization directions of the magnetic field can be found where the ellipticity of the resulting electric field is small. Although the phase tensor skew angle β tells us that the situation is 3-D, the value of β is small ($< 3^\circ$). This suggests that a small value of β by itself is not necessarily a good indication of the nearness of the regional conductivity structures to 2-D. A much better indication of the inappropriateness of a 2-D analysis in this example is the rapid (10° in 0.5 km) northeast–southwest variation in the direction of the major axis of the tensor ellipse.

Relationship to Bahr's method

If the regional structure is 2-D, the direction of the principal axes of the phase tensor (α) will be the same as the strike direction given by the two most commonly used approaches to distortion analysis, Bahr (1988, 1991) and Groom & Bailey (1989, 1991). In particular, the formula for the strike direction given by Bahr can be reduced to eq. (22). Thus, in 3-D situations where β is small, Bahr's expression for the regional strike direction will be close to one of the principal axes of the phase tensor.

Bahr (1988, 1991) also proposed a dimensionless, coordinate-invariant measure of the dimensionality of the regional conductivity structure similar to β which he called the phase-sensitive skew (η). In terms of the quantities used in this paper, η is given by the expression

$$\eta^2 = 2\ \det(\mathbf{X})|\Phi_{12} - \Phi_{21}|/|Z_{12} - Z_{21}|^2. \qquad (28)$$

Note that unlike β (eq. 19), η is a function of the coordinate invariants of the *observed* impedance tensor and the phase tensor skew ($\Phi_{12} - \Phi_{21}$).

The condition $\eta = 0$ (or equivalently $\Phi_{12} - \Phi_{21} = 0$), represents the requirement that the component phases of the impedance tensor in each column of the impedance tensor matrix are equal, which is true if the regional conductivity structure is 2-D (Bahr 1988, 1991). However, if $|\Phi_{12} - \Phi_{21}| \neq 0$ the effect of a galvanic distortion on eq. (28), contained in the det($\mathbf{X}$) and $|Z_{12} - Z_{21}|^2$ terms, will

not cancel out. Thus, if the regional conductivity structure is not 2-D, the value of η will depend on whether or not the observed response is distorted. For this reason it is questionable whether the magnitude of η is a good indication of the dimensionality of the regional conductivity structure.

Any distortion analysis based on the assumption that the regional conductivity structure is 2-D cannot include the asymmetry in the MT response represented by the phase tensor skew angle (β). In what is, in essence, an attempt to represent this asymmetry, Bahr (1991) introduced a *complex* parameter (the phase deviation) into the distortion tensor while retaining the 2-D form for the regional impedance tensor. This parametrization is inconsistent with the 3-D source of the asymmetry and violates the basic physical assumption that the distortion tensor is real for a galvanic distortion. One of the advantages of the phase tensor analysis is that the asymmetry in the phase response is represented explicitly and no assumption about the form of regional impedance tensor is required.

Relationship to Groom–Bailey decomposition

In this (Groom & Bailey 1989, 1991) and other similar approaches (Zhang *et al.* 1987; Chakridi *et al.* 1992; Chave & Smith 1994; Smith 1995) to distortion analysis the observed impedance tensor is decomposed into a 2-D regional impedance tensor $\mathbf{Z}'_{\mathrm{R}}$ and a (real) distortion tensor $\mathbf{D}'$, which is parametrized in different ways by different authors. The observed impedance tensor $\mathbf{Z}$ can therefore be expressed by the relation

$$\mathbf{Z} = \mathbf{R}(\theta)[\mathbf{D}'\mathbf{Z}'_{\mathrm{R}}]\mathbf{R}^{\mathrm{T}}(\theta), \tag{29}$$

where $\mathbf{Z}'_{\mathrm{R}}$ is the 2-D (anti-diagonal) impedance tensor (eq. 24) and θ is the (unknown) strike of the conductivity structure. Eq. (29) has a total of nine unknowns θ, $X_\perp$, $Y_\perp$, $X_\parallel$, $Y_\parallel$ and the four components of $\mathbf{D}'$. The number of measured quantities in $\mathbf{Z}$ is eight (i.e. the components of $\mathbf{X}$ and $\mathbf{Y}$) so eq. (29) is underdetermined. Groom & Bailey (1989, 1991) factorize the distortion tensor into three, linearly independent, 2×2 matrices and a scalar, i.e.

$$\mathbf{D} = \mathbf{gTSA} \tag{30}$$

where

$$\mathbf{T} = \frac{1}{\sqrt{1+t^2}}\begin{bmatrix} 1 & -t \\ t & 1 \end{bmatrix}, \quad \mathbf{S} = \frac{1}{\sqrt{1-e^2}}\begin{bmatrix} 1 & e \\ e & 1 \end{bmatrix},$$
$$\mathbf{A} = \frac{1}{\sqrt{1-s^2}}\begin{bmatrix} 1+s & 0 \\ 0 & 1-s \end{bmatrix} \tag{31}$$

and g, the 'site gain', is a scalar. That is Groom & Bailey rewrite eq. (29) as

$$\mathbf{Z} = \mathbf{R}(\theta)[g\mathbf{TSAZ}'_{\mathrm{R}}]\mathbf{R}^{\mathrm{T}}(\theta). \tag{32}$$

In essence, the four unknown components of $\mathbf{D}'$ have been rewritten in terms of the (unknown) parameters: g, t, e and s. These parameters cannot be determined from the observed impedance tensor without independent information or assumptions.

Since the operation of g and $\mathbf{A}$ on $\mathbf{Z}'_{\mathrm{R}}$ is equivalent to a non-determinable scale change or gain (say $\tilde{g}_\perp$ and $\tilde{g}_\parallel$) for each of the off-diagonal (non-zero) components of $\mathbf{Z}'_{\mathrm{R}}$, eq. (32) can be reduced to the form

$$\mathbf{Z} = \mathbf{R}(\theta)[\mathbf{TS}\tilde{\mathbf{Z}}'_{\mathrm{R}}]\mathbf{R}^{\mathrm{T}}(\theta), \tag{33}$$

where $\tilde{\mathbf{Z}}'_{\mathrm{R}}$ is the scaled version of $\mathbf{Z}'_{\mathrm{R}}$ (Groom & Bailey 1989, 1991). This reduction implicitly introduces a pair of constraint equations ($g = 1$ and $s = 0$) for the components of $\mathbf{D}$, which reduce the number of unknowns by two. The seven unknown parameters in eq. (33) (i.e. $\tilde{g}_\perp Y_\perp$, $\tilde{g}_\parallel Y_\parallel$, t, e, and θ) and thus the regional phases ($Y_\perp/X_\perp$ and $Y_\parallel/X_\parallel$) can then be determined at each period from what is now an overdetermined problem. As emphasized by McNeice & Jones (2001) one of the attractive features of the Groom–Bailey approach is that it allows a stable estimate of the strike direction to be recovered from a distorted 2-D impedance tensor that contains noise. However, as was first shown by Bahr (1988) and by the phase tensor analysis, the strike direction of a 2-D conductivity distribution can be obtained directly from the observed impedance tensor (eq. 22) without decomposition, i.e. without attempting to recover information about the structure of the distortion tensor. In practice, where the situation may only be approximately 2-D, the strike angle recovered by Groom–Bailey decomposition will depend on how the asymmetry in the regional response is distributed into the misfit.

Other parametrizations of the distortion tensor are equally plausible. For example, the distortion tensor could be represented by its SVD i.e.

$$\mathbf{D} = \mathbf{R}^{\mathrm{T}}(\alpha_{\mathrm{D}} - \beta_{\mathrm{D}})\begin{bmatrix} d_{\max} & 0 \\ 0 & d_{\min} \end{bmatrix}\mathbf{R}(\alpha_{\mathrm{D}} + \beta_{\mathrm{D}}), \tag{34}$$

where β_{D} and the principal values ($d_{\max}$ and $d_{\min}$) are coordinate invariant and α_{D} is the coordinate dependent angle corresponding to eq. (22). Like the Groom–Bailey parameters, the SVD parameters of $\mathbf{D}$ are functions of the distortion tensor components and cannot be determined from the observed impedance without auxiliary information. By assuming a 2-D form for the regional impedance tensor (with strike direction determined from the principal axes of the phase tensor) and introducing constraints on the distortion tensor we can solve for the SVD parameters of $\mathbf{D}$ in a similar way to how Groom & Bailey (1989, 1991) solve for $\mathbf{T}$ and $\mathbf{S}$.

One of the less satisfactory features of the Groom–Bailey approach is that only one of the two constraints used for the decomposition is coordinate invariant. Other choices of constraint are possible and equally plausible. In particular both constraints can be chosen to be coordinate invariant. However, it is important to stress that the choice of constraint partially determines the values of the distortion parameters recovered and thus limits their physical significance. We will discuss the analysis of the distortion tensor in more detail elsewhere.

FIELD EXAMPLE

To demonstrate the application of the phase tensor to a real data set we have analysed data from a MT survey conducted in the Taupo Volcanic Zone (TVZ) in the North Island of New Zealand. Phase tensor ellipses from this survey are shown in Fig. 7 superimposed on a gravity map of the region. Details of the collection and interpretation of these data using conventional techniques (i.e. techniques based on a 2-D model of the regional conductivity structure) are given in Ogawa *et al.* (1999).

The central part of the TVZ shown in Fig. 7 is characterized by northwest–southeast extension and late Pliocene to Quaternary rhyolitic volcanism (Wilson *et al.* 1995). This has resulted in the formation of a large volcano-tectonic depression filled with low-density volcaniclastic sediments and the central part of the TVZ can be identified with the area of low gravity (say <20 mGal) in Fig 7 (Bibby *et al.* 1995). The volcaniclastic sediments are much more conductive (~3–30 Ω m) than the underlying basement rocks (~1000 Ω m) or the layer of recent volcanics (100–1000 Ω m) that covers the entire region. Thus where the basement is close to the

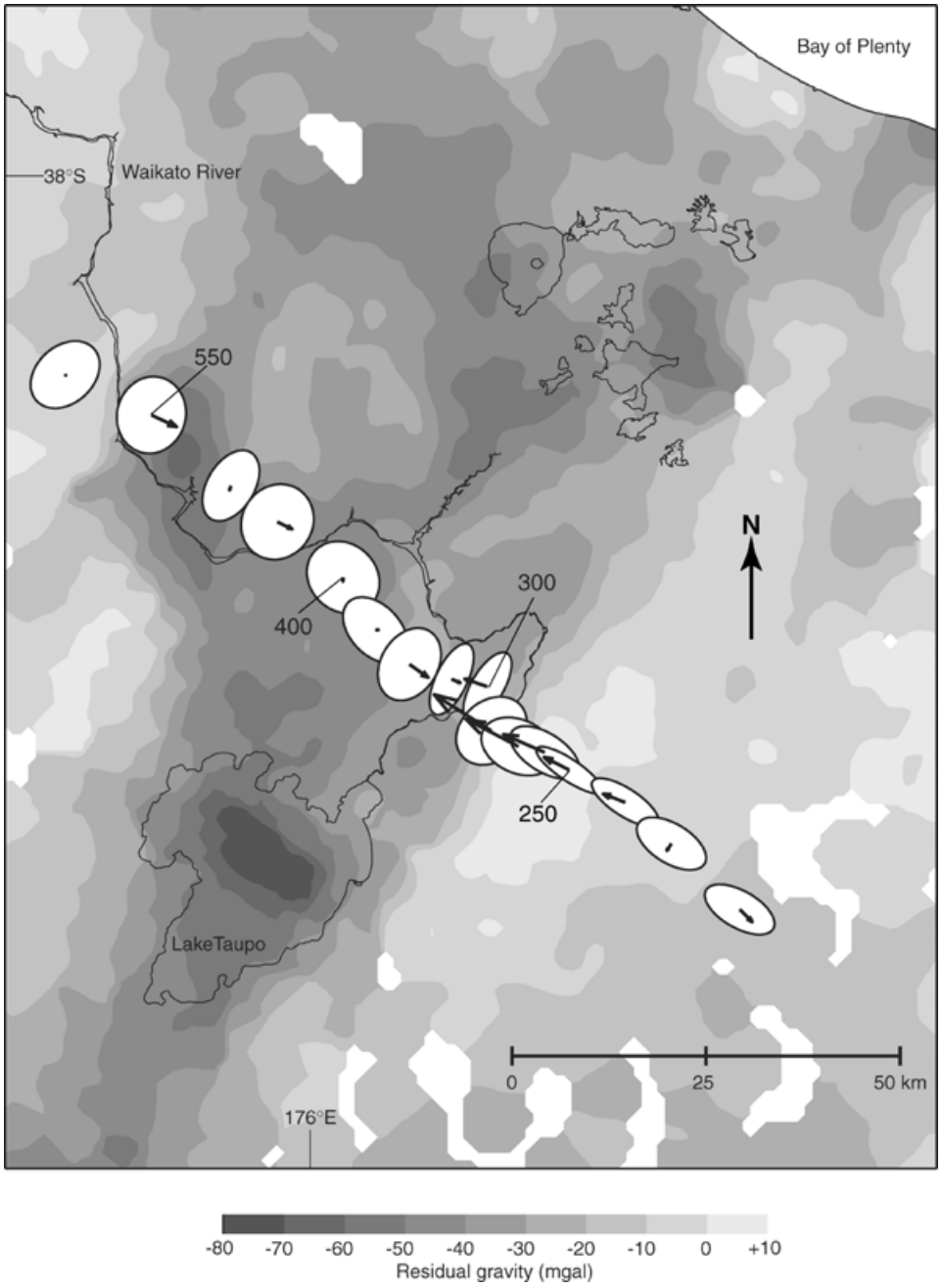

Figure 7. Phase tensor ellipses at $T = 21.3$ s superimposed on the regional gravity map of the Taupo Volcanic Zone (after Bibby *et al.* 1995). The ellipses have been drawn so that the major axes are all the same length. Also shown are the corresponding induction arrows (real part).

surface (in the west and southeast) the conductivity structure of the upper part of the crust will reflect the structure shown by the gravity map (Fig. 7).

Estimates of the Groom–Bailey strike direction for the measurement sites shown in Fig. 7 are concentrated between N40°E and N50°E suggesting that the overall conductivity structure is approximately 2-D (Ogawa *et al.* 1999). We have also analysed these data using the multisite Groom–Bailey decomposition technique published by McNeice & Jones (2001). This analysis gives an overall apparent strike direction of N43.5°E ± 1° in good agreement with the N45°E strike direction used by Ogawa *et al.* (1999).

As can be seen in Fig. 7, the southeastern margin of the TVZ is marked by an almost linear northeast–southwest gravity gradient. The major axes of the phase tensor ellipses near this margin are oriented parallel and perpendicular to the strike of the gravity gradient similar to the behaviour expected for a 2-D conductivity distribution. Independent evidence for the 2-D nature of the conductivity structure along this margin is provided by detailed long-offset DC resistivity surveys (Bibby *et al.* 1998) and by the behaviour of the induction arrows shown in Fig. 7. In a 2-D situation, the induction arrows will be perpendicular to the strike of the conductivity distribution and the agreement between the directions of the induction arrows and ellipse axes near the southeastern margin of the TVZ is good.

In Fig. 8 we have plotted the phase tensor properties as functions of period for four of the measurement sites shown in Fig. 7. Also

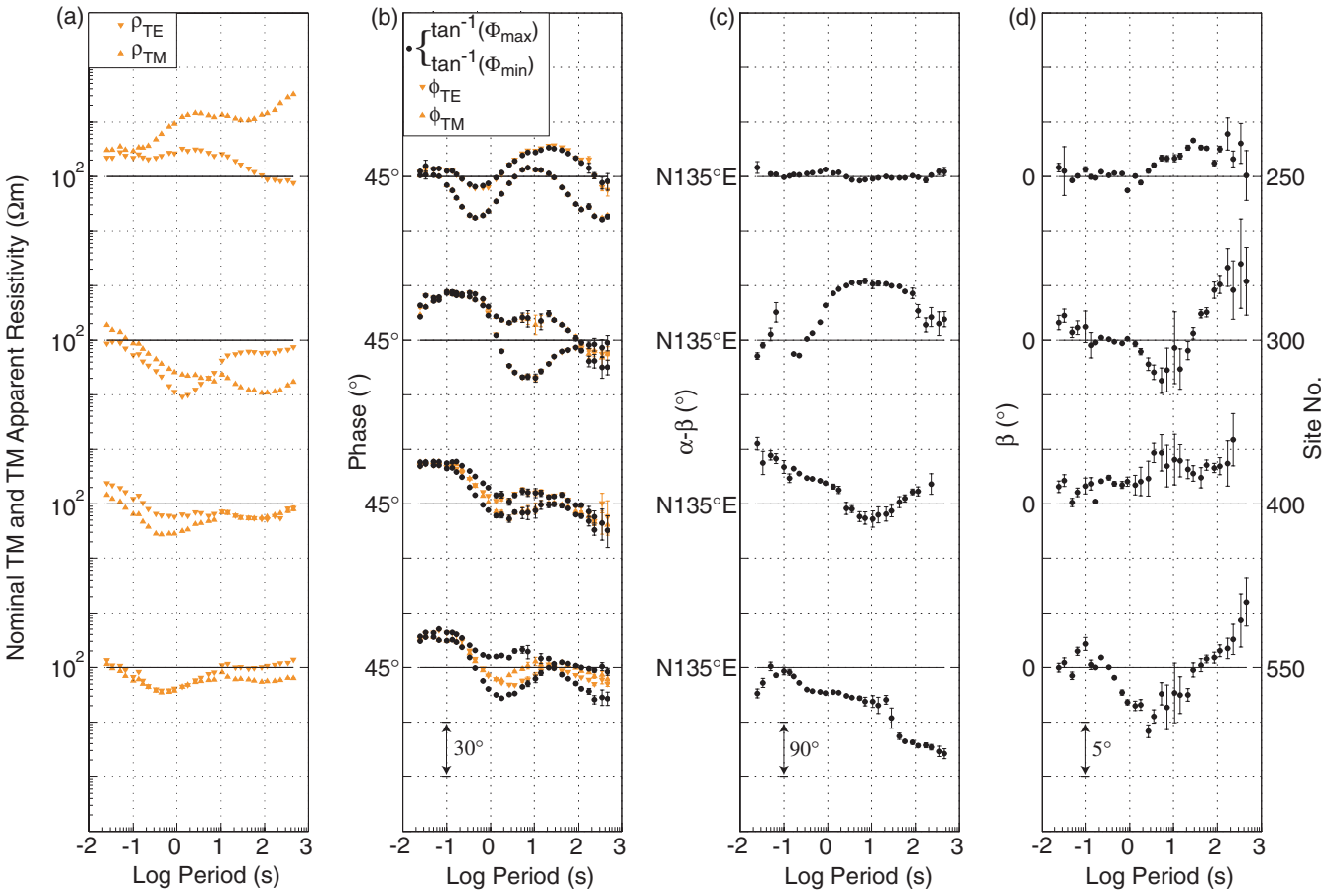

Figure 8. Apparent resistivity and phase tensor properties plotted as functions of period for measurement sites 250, 300, 400 and 550 (locations shown in Fig. 7). The error bars show the standard error calculated from the variances of the measured impedance tensor components. (a) Nominal TE and TM mode apparent resistivity sounding curves. (b) Phase tensor principal values [i.e. $\tan^{-1}(\Phi_{max})$ and $\tan^{-1}(\Phi_{min})$] superimposed onto a plot of the TE and TM mode phases with respect to N45°E. (c) Direction of the phase tensor major axis with respect to N135°E. At periods where the error bars of Φ_{max} and Φ_{min} overlap in (b) the response is assumed to be 1-D and corresponding points in (c) are not plotted. Points in (b) and (c) for which the standard error is >30° have been omitted. (d) Phase tensor skew angle β. Where the standard error of the skew angle is >5° the point has been omitted.

shown (Fig. 8a) are the ρ_{xy} and ρ_{yx} apparent resistivities (proportional to $|Z_{xy}|^2$ and $|Z_{yx}|^2$) in a Cartesian coordinate system with its x-axis aligned N45°E. That is ρ_{xy} and ρ_{yx} are (respectively) the nominal TE and TM apparent resistivities with respect to the southeastern margin of the TVZ. At the three sites within the TVZ (i.e. sites 300, 400 and 550) the apparent resistivity curves have a well-developed minimum reflecting the underlying conductive sediments. This minimum is absent at site 250 outside the TVZ where the resistive basement rocks are close to the surface. For periods <0.3 s, the TM and TE apparent resistivity curves (Fig. 8a) at sites 300 and 400 appear to be displaced by a constant factor with respect to each other. This suggests that the data at these two sites have been distorted.

In Fig. 8(b) we have superimposed the principal values of the phase tensor (i.e. $\tan^{-1}\Phi_{min}$ and $\tan^{-1}\Phi_{min}$) on plots of the (nominal) TE and TM phases. For the two southeastern sites (250 and 300) the differences between the principal phase values and the TE and TM phases at periods <100 s are small, indicating that the conductivity structure in this area is approximately 2-D with a strike of N45°E. However, significant differences between the principal phase values and the TE and TM phases are present at sites 400 and 550. This difference suggests that either 3-D effects are present or that the strike direction has been chosen incorrectly. At sites 400 and 550, the directions of the principal axes change with period, implying that the regional conductivity structure in the neighbourhood of these two sites is 3-D. Plots of the skew angle β (Fig. 8d) for these sites support this inference.

For the two southeastern sites (250 and 300), the variation in the direction of the major axis of the phase tensor (Fig. 8c) is <15° in the period range between 1 and 100 s, consistent with a quasi 2-D regional structure near the southeastern margin of the TVZ. The variation is larger at site 300 where the skew angle also changes by a total of about 7° over the same period range. At greater periods >100 s, the principal direction at site 300 changes by about 45° so that one interpretation of the response at this site is that the effect of a distant, off-strike structure becomes significant at periods >100 s. Indeed, the directions of the principal axes from all the sites within the TVZ (not all shown in Fig. 8) vary significantly in this period range. At the sites southeast of the TVZ (of which site 250 is one example), the principal directions show much less variation and are coherent between sites. It is clear from the phase tensor analysis that the conductivity structure within the TVZ is 3-D and a 3-D approach to data collection and analysis will be required to more clearly resolve the conductivity structure.

CONCLUSIONS

One of the difficulties of interpreting MT data is that the information from deeper levels is distorted by the effect of near-surface conductivity heterogeneities. The traditional approach to this difficulty has been to assume a simplified 2-D structure for the underlying regional conductivity distribution. This assumption allows the regional phase information and strike of a 2-D conductivity distribution to be derived from a distorted set of observations, provided the distortion is galvanic. We have shown that the 2-D assumption is unnecessary and that the phase relationship between the horizontal components of the electric and magnetic fields may be derived directly from the observed impedance tensor in situations where the regional conductivity structure is 3-D. In essence we have generalized the representation of the MT phase so that it applies in the 3-D case, where the electric field response to a linearly polarized magnetic field is (in general) elliptically polarized. This representation takes the form of a (second-rank) tensor that is unaffected by a galvanic distortion of the electric field, consistent with the physical behaviour expected for the MT phase.

The phase tensor components and their associated three coordinate invariants are simple functions of the observed impedance tensor components. Graphically, the tensor can be represented as an ellipse where the principal axes of the tensor are represented by the major and minor axes of the ellipse. The third coordinate invariant, the skew angle, is a measure of the asymmetry in the regional MT response. In 2-D the phase tensor is symmetric and the skew angle is zero. While a large value of the skew angle necessarily implies a 3-D regional conductivity structure, our results suggest that a small value of the skew angle is not necessarily a good indication of the nearness of the conductivity structure to 2-D. Much more reliable criteria for two-dimensionality are the constancy of the direction of the principal axes of the phase tensor with period and with location along strike.

Our modelling results suggest that the direction of the phase tensor major axis indicates the preferred flow direction of the regional induction current. Maps of the phase tensor ellipses at different periods provide a simple way of depicting this direction and thus (indirectly) of visualizing lateral changes in the regional conductivity structure at different depths. Such maps will not be influenced by near-surface galvanic effects.

Spatial and temporal variations in the near-surface conductivity distribution dominate the measured amplitudes in MT surveys designed to monitor temporal conductivity changes at deeper levels. Provided the effect of any temporal change in the near-surface conductivity can be represented by a galvanic distortion of the electric field, any change in the phase tensor will reflect only the conductivity variations at deeper levels. Detecting conductivity changes at depth is potentially an important future application of this method of analysis.

The calculation of the phase tensor requires no assumption about the dimensionality of the underlying conductivity distribution and is applicable where both the heterogeneity and the regional conductivity structures are 3-D. Although we have introduced the phase tensor in the context of the galvanic distortion problem, the representation of the MT phase as a tensor is not restricted to this context. Rather, the phase tensor should be considered to be a fundamental property of the impedance tensor expressing how the phase relationship between the electric and magnetic field changes with polarization in situations where the conductivity structure is 3-D.

ACKNOWLEDGMENTS

Much of this work would not have been possible without access to the 3-D EM modelling code developed by Zonghou Xiong. We would also like to thank Gary McNeice and Alan Jones for making their multisite Groom–Bailey code available. Reviews by John Booker, Wolfgang Soyer and Martyn Unsworth helped us to clarify a number of ideas in the paper. Mark Berdichevsky and John Weaver also commented on an earlier version of this paper. The MT data from the Taupo Volcanic Zone were collected in a joint project between the Institute of Geological and Nuclear Sciences in New Zealand and the Geological Survey of Japan. We would especially like to acknowledge the contribution of our Japanese colleagues Yasuo Ogawa (now at the Tokyo Institute of Technology), Shinichi Takakura, Toshihiro Uchida, Nobuo Matsushima, Toshiyuki Tosha and Yuji Nishi for making that project and on going work in the Taupo Volcanic Zone so successful. This work was supported by the Marsden Fund administered by the Royal Society of New Zealand (Institute of Geological and Nuclear Sciences contribution 2902) and by the Enterprise Ireland Basic Research Grants Scheme (project SC-1998-501).

REFERENCES

Bahr, K., 1988. Interpretation of the magnetotelluric tensor: regional induction and local telluric distortion, *J. Geophys.,* **62,** 119–127.

Bahr, K., 1991. Geological noise in magnetotelluric data: a classification of distortion types, *Phys. Earth planet. Inter.,* **66,** 24–38.

Bibby, H.M., 1986. Analysis of multiple-source bipole-dipole resistivity surveys using the apparent resistivity tensor., *Geophysics,* **51,** 972–983.

Bibby, H.M., Caldwell, T.G., Davey, F.J. & Webb, T.H., 1995. Geophysical evidence on the structure of the Taupo Volcanic Zone and its hydrothermal circulation, *J. Volcanol. Geotherm. Res.,* **68,** 29–58.

Bibby, H.M., Caldwell, T.G. & Risk, G.F., 1998. Electrical resistivity image of the upper crust within the Taupo Volcanic Zone, New Zealand, *J. geophys. Res.,* **81,** 69–89.

Bruton, P., 1994. Analysis of broadband magnetotelluric data and an application to the Irish Variscides, *PhD Thesis*, National University of Ireland, Galway.

Caldwell, T.G. & Bibby, H.M., 1998. The instantaneous apparent resistivity tensor: a visualisation scheme for LOTEM electric field measurements, *Geophys. J. Int.,* **135,** 817–834.

Caldwell, T.G., Bibby, H.M. & Brown, C., 2002. Controlled source apparent resistivity tensors and their relationship to the magnetotelluric impedance tensor, *Geophys. J. Int.,* **151,** 755–770.

Chakridi, R., Chouteau, M. & Mareschal, M., 1992. A simple technique for analysing and partly removing galvanic distortion from the magnetotelluric impedance tensor: application to Abitibi and Kapuskasing data (Canada), *Geophys. J. Int.,* **108,** 917–929.

Chave, A.D. & Smith, J.T., 1994. On electric and magnetic galvanic distortion tensor decompositions, *J. geophys. Res.,* **99**(B3), 4669–4682.

Groom, R.W. & Bahr, K., 1992. Corrections for near surface effects: Decomposition of the magnetotelluric impedance tensor and scaling corrections for regional resistivities: a tutorial, *Surv. Geophys.,* **13,** 341–379.

Groom, R.W. & Bailey, R.C., 1989. Decomposition of the magnetotelluric tensors in the presence of local three-dimensional galvanic distortion, *J. geophys. Res.,* **94,** 1913–1925.

Groom, R.W. & Bailey, R.C., 1991. Analytical investigations of the effects of near surface three-dimensional galvanic scatterers on MT tensor decomposition, *Geophysics,* **56,** 496–518.

Jiracek, G.R., 1990. Near-surface and topographic distortions in electromagnetic induction, *Surv. Geophys.,* **11,** 163–203.

McNeice, G.W. & Jones, A.G., 2001. Multisite, multifrequency tensor decomposition of magnetotelluric data, *Geophysics,* **66,** 158–173.

Ogawa, Y. *et al.*, 1999. Magnetotelluric measurements across the Taupo Volcanic Zone, New Zealand—preliminary results, *Geophys. Res. Lett.,* **26,** 3673–3676.

Parkinson, W.D., 1962. The influence of continents and oceans on geomagnetic variations, *Geophys. J. R. astron. Soc.,* **6,** 441–449.

Press, W.H., Flannery, B.P., Teukolsky, S.A. & Vetterling, W.T., 1986. *Numerical Recipes—the Art of Scientific Computing,* Cambridge University Press, Cambridge.

Ritter, P., 1996. Separation of local and regional information in geomagnetic response functions using hypothetical event analysis, *PhD thesis*, University of Edinburgh.

Singer, B.S., 1992. Correction for distortions of magnetotelluric fields: limits of validity of the static approach, *Surv. Geophys.,* **13,** 309–340.

Smith, J.T., 1995. Understanding telluric distortion matrices, *Geophys. J. Int.,* **122,** 219–226.

Utada, H. & Munekane, H., 2000. On galvanic distortion of three-dimensional magnetotelluric impedances, *Geophys. J. Int.,* **140,** 385–398.

Wilson, C.J.N., Houghton, B.F., McWilliams, M.O., Lanphere, M.A., Weaver, S.D. & Briggs, R.M., 1995. Volcanic and structural evolution of the Taupo Volcanic Zone, New Zealand: a review, *J. Volcanol. Geotherm. Res.,* **68,** 1–28.

Xiong, Z., 1992. Electromagnetic modelling of three-dimensional structures by the method of system iteration using integral equations, *Geophysics,* **57,** 1556–1561.

Xiong, Z. & Tripp, A., 1995. A block iterative algorithm for 3D electromagnetic modelling using integral equations with symmetrized substructures, *Geophysics,* **60,** 291–295

Zhang, P., Roberts, R.G. & Pedersen, L.B., 1987. Magnetotelluric strike rules, *Geophysics,* **52,** 267–278.

APPENDIX

PHASE TENSOR COORDINATE INVARIANTS

Expressions for the coordinate invariants of a (non-symmetric) second-rank 2-D tensor can be found in Bibby (1986) and are summarized here for completeness. Writing the phase tensor as the matrix

$$\mathbf{\Phi} = \begin{bmatrix} \Phi_{11} & \Phi_{12} \\ \Phi_{21} & \Phi_{22} \end{bmatrix} \tag{A1}$$

the simplest algebraic representations of the tensor invariants are the trace

$$\mathrm{tr}(\mathbf{\Phi}) = \Phi_{11} + \Phi_{22}, \tag{A2}$$

the skew

$$\mathrm{sk}(\mathbf{\Phi}) = \Phi_{12} - \Phi_{21} \tag{A3}$$

and the determinant

$$\det(\mathbf{\Phi}) = \Phi_{11}\Phi_{22} - \Phi_{12}\Phi_{21} \tag{A4}$$

of the matrix. Note that the determinant is a quadratic function of the tensor components.

It is convenient to re-express all the invariants as the first order functions:

$$\Phi_1 = \mathrm{tr}(\mathbf{\Phi})/2 \tag{A5}$$

$$\Phi_2 = [\det(\mathbf{\Phi})]^{1/2} \tag{A6}$$

and

$$\Phi_3 = \mathrm{sk}(\mathbf{\Phi})/2. \tag{A7}$$

In terms of these quantities the maximum, minimum and skew angle (eq. 19) are given by the expressions:

$$\Phi_{\min} = \left(\Phi_1^2 + \Phi_3^2\right)^{1/2} - \left(\Phi_1^2 + \Phi_3^2 - \Phi_2^2\right)^{1/2} \tag{A8}$$

$$\Phi_{\max} = \left(\Phi_1^2 + \Phi_3^2\right)^{1/2} + \left(\Phi_1^2 + \Phi_3^2 - \Phi_2^2\right)^{1/2} \tag{A9}$$

$$\beta = \frac{1}{2}\tan^{-1}\left(\frac{\Phi_3}{\Phi_1}\right). \tag{A10}$$

The fourth SVD parameter α (eq. 22), which is needed to complete the specification of the tensor, is not coordinate invariant and cannot be expressed as a function of the coordinate invariants alone.

Note that we have tacitly assumed in eq. (A6) that $\det(\mathbf{\Phi}) \geq 0$. If the conductivity distribution is very unusual and 3-D it is possible that the $\det(\mathbf{\Phi})$ may vanish or become negative. In the singular case ($\det(\mathbf{\Phi}) = 0$) the expressions (eqs A8 and A9) for $\Phi_{\max}$ and $\Phi_{\min}$ are well-defined and $\Phi_{\min} = 0$. That is the phase tensor ellipse has zero area and the tensor is represented by a line of length $2\Phi_{\max}$. If $\det(\mathbf{\Phi}) < 0$ then we can retain eq. (A8) by defining $\Phi_2 = |\det(\mathbf{\Phi})|^{1/2}$ and assign a negative sign to the value of $\Phi_{\min}$. The behaviour of the phase tensor in this unusual situation can be envisaged graphically. Assume that the effect of the conductivity distribution is insignificant at some period and that $\Phi_{\max}$ and $\Phi_{\min}$ are >0. As the unusual 3-D effects become important, the minor axis of the tensor ellipse shrinks. Eventually, the effect of the conductivity structure causes the ellipse to shrink down to a line (length $2\Phi_{\max}$) where $\Phi_{\min}$ and $\det(\mathbf{\Phi})$ are both zero. As these effects increase the ellipse will re-expand, although now $\Phi_{\min}$ and $\det(\mathbf{\Phi})$ are negative.

Tensor ellipse

The angle $\alpha - \beta$ defines direction of the major axis of the tensor ellipse in the Cartesian coordinate system used to express the tensor. Knowing the orientation of the major axis the ellipse may then be constructed from knowledge of the lengths of the major and minor axes (i.e. from $\Phi_{\max}$ and $\Phi_{\min}$). A more direct and simpler way of drawing the tensor ellipse is to recall that the matrix representing the tensor can be thought of as mapping of one vector into another. By generating a set of unit vectors at say 1° intervals around a circle and transforming each unit vector with the tensor matrix the resultant (transformed) set of vectors define the tensor ellipse. This is easily and compactly implemented in modern computer languages such as MATLAB.